

GIFStream: 4D Gaussian-based Immersive Video with Feature Stream

Hao Li, Sicheng Li, Xiang Gao, Abudouaihati Batuer, Lu Yu**, Yiyi Liao*
Zhejiang University

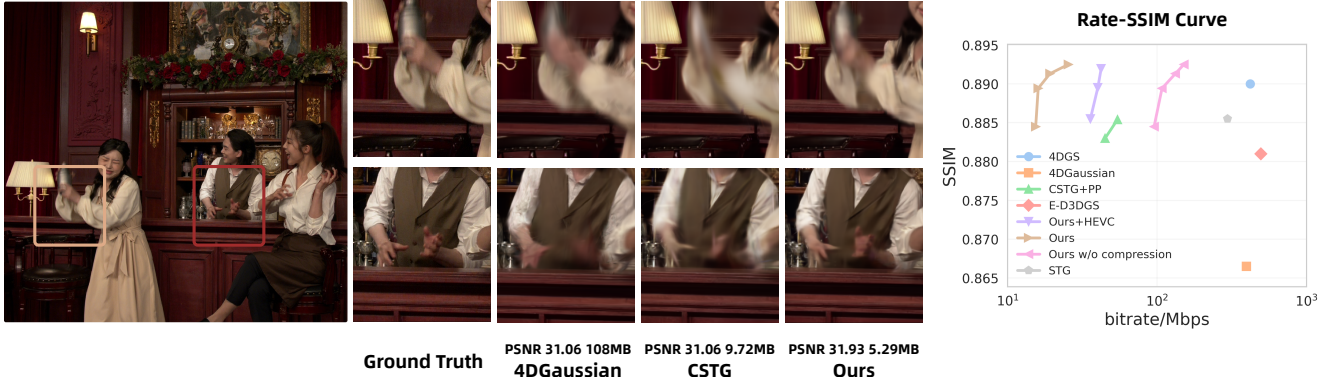


Figure 1. **GIFStream** achieves high quality and small storage size on dynamic scenes containing fast motion. We present the rendering results on a challenging scene on the left and the Rate-SSIM curve on the right.

Abstract

Immersive video offers a 6-Dof-free viewing experience, potentially playing a key role in future video technology. Recently, 4D Gaussian Splatting has gained attention as an effective approach for immersive video due to its high rendering efficiency and quality, though maintaining quality with manageable storage remains challenging. To address this, we introduce GIFStream, a novel 4D Gaussian representation using a canonical space and a deformation field enhanced with time-dependent feature streams. These feature streams enable complex motion modeling and allow efficient compression by leveraging temporal correspondence and motion-aware pruning. Additionally, we incorporate both temporal and spatial compression networks for end-to-end compression. Experimental results show that GIFStream delivers high-quality immersive video at 30 Mbps, with real-time rendering and fast decoding on an RTX 4090. Project page: <https://xdimlab.github.io/GIFStream>

1. Introduction

Immersive video, which enables users to explore dynamic scenes with six degrees of freedom (6-DoF), offers a highly engaging experience with applications in virtual meetings, sports viewing, and gaming. Recently, 3D Gaussian splat-

ting (3DGS) [15] and its 4D extensions have emerged as promising approaches for immersive video, achieving high-quality reconstruction and real-time rendering performance. However, to make these technologies feasible for real-world applications, it is essential to balance *rendering quality* with *storage requirements*. Although 4D Gaussian representations show promise for immersive video, current techniques struggle to achieve this balance effectively.

To tackle this challenge, we argue that both the *representation* and *compression* should be considered together. An ideal 4D representation should support high-quality novel view synthesis for dynamic scenes while allowing for efficient compression. One line of works, as shown in Fig. 2 left, represents the 4D scene as a 3D canonical space combined with a deformation field, parameterized by models such as MLPs, triplanes, per-frame single embedding or deformation bases [1, 11, 13, 16, 41, 43]. Since the deformation field is generally lightweight, compact memory usage can be achieved by applying 3D compression methods to the canonical space. However, deformation-based methods struggle with highly dynamic scenes, as existing deformation representations lack the capacity to capture rapid motion. Another line of works [6, 23, 42], shown in Fig. 2 middle, employs 4D Gaussians to represent the scene, where each primitive models a local spatial region across a brief temporal segment. This allows for high-quality representation of complex motion using numerous 4D Gaussian primitives, though at the cost of substantial memory consump-

* Corresponding author. ** Co-corresponding author.

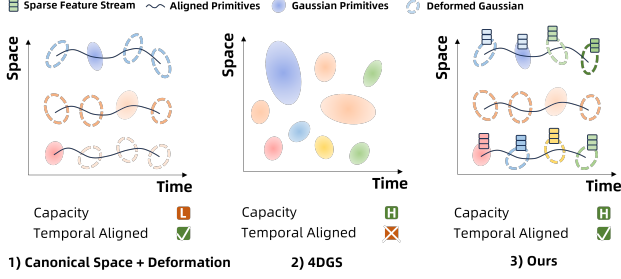


Figure 2. **Comparison of 4D Representations.** 1) Deformation-based representation stores a 3D Gaussian in a canonical space and its deformation along a long time horizon. and 2) 4D Gaussian representation which models a windowed spacetime region. We propose 3) GIFStream by adding time-dependent feature streams on top of deformation-based representation, improving its capacity while maintaining temporal alignment for efficient compression.

tion. Moreover, the 4D Gaussian primitives are discretely distributed across the 4D space, lacking correspondences between different primitives. This limits compression efficiency, since temporal redundancies could not be effectively eliminated without temporal correspondence.

In this work, we introduce **GIFStream**, a representation that captures highly dynamic content while enabling efficient temporal compression. Our key idea is to incorporate an adaptive sparse feature stream into deformation-based methods, enhancing their ability to model complex motion while enabling efficient immersive video compression through the inherent temporal correspondence as shown in Fig. 2 right. Our canonical space consists of a set of anchor points following Scaffold-GS [25]. And the key to GIFStream is that each anchor consists of a time-independent feature and a time-dependent feature stream, both are combined to predict time-dependent 3D Gaussian primitives at various timestamps, facilitating the capture of fast motion. While adding the feature streams increases the parameter size, they are learned in a motion-adaptive manner and hence can be easily pruned for static regions. Furthermore, it allows for efficient compression by leveraging the temporal correspondence information. To effectively compress the whole representation, we sort both time-independent and time-dependent features into two distinct video sequences, enabling the application of different video codecs including HEVC and learning-based methods. For optimal compression efficiency, we train our representation with quantization aware training and jointly train an autoregressive entropy estimation network to conduct End-to-End compression.

To evaluate GIFStream, we conducted experiments on several challenging dynamic datasets, comparing our method with other 4D representation and compression techniques. The results indicate that GIFStream can efficiently

represent highly dynamic 1080p immersive videos at a bit rate of 30 Mbps, which is comparable to that of 4K 2D videos. Furthermore, GIFStream achieves an optimal balance between quality and storage requirements, while enabling fast decoding and rendering on the RTX 4090 GPU.

2. Related Work

NeRF-based Dynamic Novel View Synthesis: Synthesizing novel views of a dynamic scene is a challenging task. Inspired by the success of the Neural Radiance Field (NeRF) [28], several approaches attempt to extend it to dynamic scenes. Deformation-based works [22, 32] construct deformation field to adjust the sampled query points for a specific time. Kplanes [9] and Hexplanes [4] propose to directly construct 4D feature space and query the corresponding feature for specific time and space positions. Nerf-player [35] combines the two by deforming a static field and add a time variable field like the second line. This combination improves the ability to capture new elements compared to pure deformation methods while also reducing redundancy. Inspired by NeRFPlayer, we propose incorporating time-dependent features to predict 3D Gaussian primitives at each timestamp, achieving higher quality while maintaining small storage requirements by further exploiting compression techniques.

3DGS-based Dynamic Novel View Synthesis: As 3D Gaussian Splatting achieves great quality and rendering speed, similar ideas are applied to extend 3D Gaussian Splatting to dynamic scenes. 4D Gaussian Splatting (4DGS) methods [6, 23, 42] keep Gaussian primitives in 4D space, with each primitive capturing a localized period in time and space. As illustrated in Fig. 2, these methods can be viewed as 3D Gaussian spanned over learned time periods. This yields a high capability to model dynamic scenes but at the cost of large storage. Another line of work [1, 11, 13, 16, 41, 43], as illustrated in Fig. 2 left, basically applies deformation idea. The long-term tracking for all frames reduces the temporal redundancy but faces challenges in modeling complex dynamic content due to limitations in the deformation field’s capacity. Our representation demonstrates a greater ability to capture dynamic scenes compared to existing deformation methods, and it is more compression-friendly than 4DGS due to its temporally aligned structure.

Compression for NeRF-based Methods: NeRF has emerged as a promising solution for immersive video, leveraging compression techniques to balance quality and storage efficiency effectively. Related works consistently integrate quantization, transform coding, and entropy coding methods to optimize compression performance. Early efforts focused primarily on static scenes. VQAD, Masked

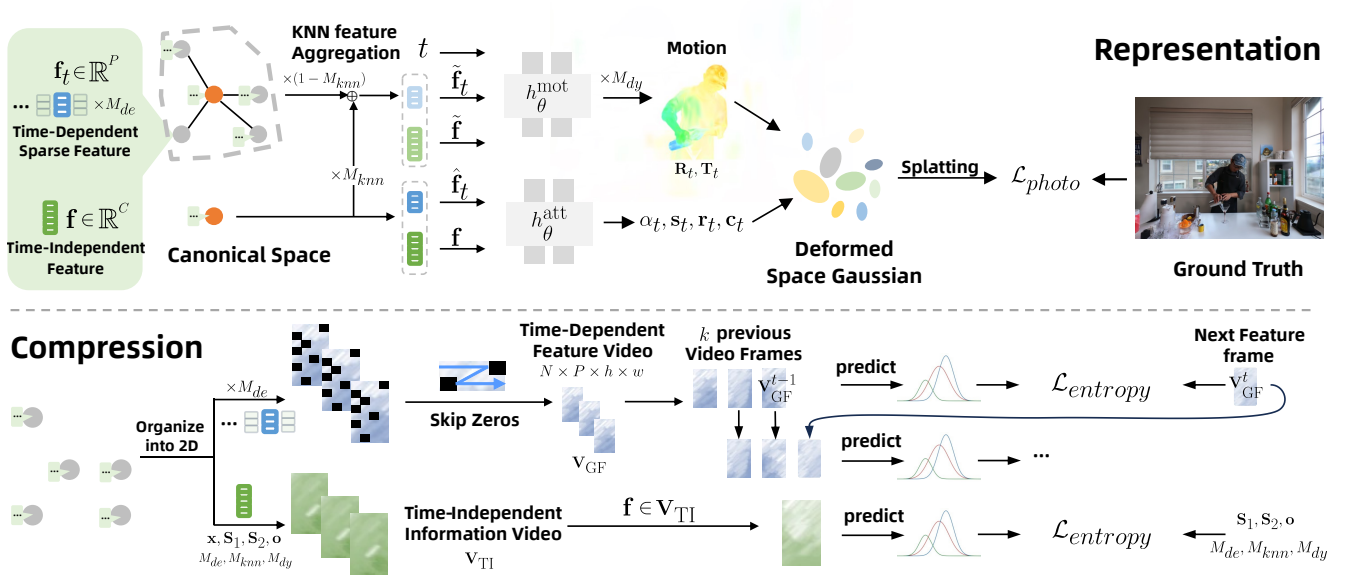


Figure 3. **Method.** (I. **Representation**) We propose enhancing deformation-based dynamic Gaussian representation using time-dependent feature streams. We attach time-dependent feature \mathbf{f}_t and time-independent feature \mathbf{f} to a set of anchor points. These features are aggregated to decode deformation motion $\mathbf{R}_t, \mathbf{T}_t$ and Gaussian attribute $\alpha_t, s_t, \mathbf{r}_t, \mathbf{c}_t$ at a specific timestamp t through MLPs. Finally, we render the target view through splatting. (II. **Compression**) For compression, we reorganize both time-dependent and time-independent parameters into two videos. The feature streams are first pruned and then compressed in an auto-regressive manner, effectively leveraging the temporal correspondence information. During training, we jointly optimize the rendering loss $\mathcal{L}_{\text{photo}}$ and add an entropy constraint $\mathcal{L}_{\text{entropy}}$.

Wavelet NeRF, and BIRF [33, 34, 37] introduce scalar quantization or vector quantization during training, while VQRF [20] applies quantization as the post-training process. Masked Wavelet NeRF and NeRFCodec [21] utilize DCT transform or VAE-based transform networks to improve transform coding. VQRF and Masked Wavelet NeRF additionally learn a probability model to conduct entropy coding with more accurate distribution estimation. For compressing dynamic radiance fields, ReRF and videoRF [38, 39] introduce residual radiance fields or sequential fields, leveraging temporal relationships to enhance compression. Despite achieving a small size, these NeRF-based methods struggle to achieve real-time rendering.

Compression for 3DGS-based Methods: With the significant improvements in rendering speed achieved by 3D Gaussian Splatting (3DGS), compression techniques for 3DGS-based methods have quickly emerged [5, 8, 12, 17, 29–31]. Beyond conventional quantization, transform, and entropy coding, compact 3DGS [17] and light Gaussian [8] reduce storage by pruning redundant Gaussian primitives. [29, 31] apply Morton Sort or Self-Organizing Sort to leverage spatial relationships for compression. HAC [5] proposes end-to-end compression using a binary hash feature grid as a context model. As for the dynamic Gaussian compression, CSTG [18] compresses STG using spatial compression methods. Mega [45] makes 4D Gaussian Splat-

ting more compact with deformation methods. \mathbf{V}^3 [40] trains 3DGS in a per-frame manner using a consistent number of Gaussians, which may struggle to represent new content. While they also exploit temporal correspondence for compression, this is achieved by leveraging traditional video compression. In contrast, our proposed deformation-based representation augmented by feature streams allows for modeling new content and fast motion, and we additionally consider end-to-end temporal compression.

3. Method

In this section, we introduce our methods in two parts: representation(Sec. 3.1) and compression(Sec. 3.2), with an overview provided in Fig. 3. Our representation consists of a canonical space and a deformation field augmented by time-dependent feature streams. For compression, we project both the time-dependent features and time-independent feature streams into 2D videos, enabling coding with video codecs. We train our representation with quantization-aware training combining rendering loss and entropy estimation for end-to-end compression. Additionally, 2D conventional video codecs can be applied. More details are introduced below.

3.1. 4D Scene Representation

Inspired by Scaffold-GS, we store features on a set of anchor points and decode each anchor into K Gaussian primitives using small MLP. To model dynamic scenes, we propose to store both time-independent and time-dependent features at each anchor point, and we refer to the time-dependent features as *feature streams*. At each timestamp, the Gaussians are decoded using two heads, one for attributes and one for motion, respectively.

Motion-Adaptive Feature Stream: Several works explored extending 3D Gaussian Splatting to dynamic scenes using deformation methods [1, 11, 13, 16, 41, 43]. Existing deformation-based methods primarily deform Gaussian Primitives based on positional encoding or low-dimensional feature planes. However, these methods face challenges in capturing the fine details of highly dynamic scenes, as the deformation field often lacks the capacity to handle fast motion scenarios. To solve this problem, we attach each anchor with two features: *time-independent feature* $\mathbf{f} \in \mathbb{R}^C$ and *time-dependent feature* $\mathbf{f}_t \in \mathbb{R}^P$ where t indicates the time stamps. This means each anchor has a feature with $C + N \cdot P$ channels when modeling N timestamps. While adding time-dependent features increases the number of parameters, we consider two strategies to effectively lower storage: 1) We make the time-dependent feature motion adaptive to eliminate them for static regions; and 2) We apply further compression by leveraging temporal correspondence, as detailed in Sec. 3.2.

To make the time-dependent feature motion-adaptive, we scale the feature with learnable parameters M_{de} as in Eq. 1.

$$\hat{\mathbf{f}}_t = M_{de} \cdot \mathbf{f}_t \quad (1)$$

We encourage M_{de} close to zero to avoid the meaningless deformation for the static anchors, and reduce the storage of feature streams. Our experiments demonstrate that the time-dependent features exhibit significant sparsity: in challenging scenes, approximately 30% of the anchors require retention of time-dependent features, while in simpler scenes, only about 0.3% of the anchors need to retain these features. This indicates that our representation can be effectively adapted to different scenarios.

Gaussian Attribute Prediction Head: At each timestamp t , we predict the opacity, scaling, rotation, and color of K Gaussian primitives from the anchor features with h_θ^{att} :

$$h_\theta^{\text{att}} : [\mathbf{f}; \hat{\mathbf{f}}_t] \mapsto \{\alpha_t^i, \mathbf{s}_t^i, \mathbf{r}_t^i, \mathbf{c}_t^i\}_{i=1}^K \quad (2)$$

where h_θ^{att} denotes the Gaussian attribute prediction head parameterized as small MLP. Specifically, α_t^i denotes the opacity, \mathbf{s}_t^i denotes the scaling, \mathbf{r}_t^i denotes the rotation and \mathbf{c}_t^i denotes the color of Gaussian i . Here, the \mathbf{s}_t^i is scaled by a per-anchor factor \mathbf{S}_1 following Scaffold-GS.

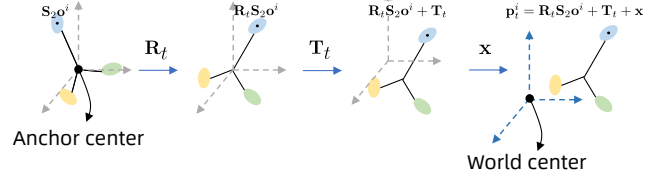


Figure 4. **Motion Illustration.** We predict the rotation and translations on the local coordinate system of the anchor.

Gaussian Motion Prediction Head: In most scenarios, the motion of the Gaussians exhibits local smoothness. To capture this local smoothness prior, we aggregate the neighboring features using K-nearest neighbors (KNN), as in Fig. 3, before decoding them to motion vectors. To further model non-smooth motion, we introduce a learnable factor M_{knn} , which enables a combination of coarse and fine motion representation:

$$\tilde{\mathbf{f}}_t = (1 - M_{knn}) \sum_{k \in \mathbb{N}} \hat{\mathbf{f}}_{k,t} + M_{knn} \hat{\mathbf{f}}_t \quad (3)$$

$$\tilde{\mathbf{f}} = (1 - M_{knn}) \sum_{k \in \mathbb{N}} \mathbf{f}_k + M_{knn} \mathbf{f} \quad (4)$$

The obtained locally smoothed feature $\tilde{\mathbf{f}}_t$ is mapped to motion combined with the time-independent feature \mathbf{f} :

$$h_\theta^{\text{mot}} : [\tilde{\mathbf{f}}; \tilde{\mathbf{f}}_t; t] \mapsto \mathbf{R}_t, \mathbf{T}_t \quad (5)$$

Here, we predict the motion $\mathbf{R}_t, \mathbf{T}_t \in SE(3)$ of each anchor considering the Gaussian Primitives are tightly attached to the anchor. To ensure that anchors representing static objects remain stationary, we attach a learnable parameter M_{dy} that modulates the scaling of motion for each anchor and apply regularization on M_{dy} . Specifically, the h_θ^{mot} predict two vectors \mathbf{q}_t and $\boldsymbol{\tau}_t$, and the motion can be computed as:

$$\mathbf{R}_t = \text{q2m}(\bar{\mathbf{q}} + M_{dy} \mathbf{q}_t) \quad (6)$$

$$\mathbf{T}_t = M_{dy} \boldsymbol{\tau}_t \quad (7)$$

where q2m indicates the quaternion to rotation matrix transform, $\bar{\mathbf{q}}$ denotes the unit quaternion.

Obtaining the motion of anchors, the position \mathbf{p}_t of generated Gaussians can be calculated as in Eq. 8, where \mathbf{o}^i is the offset of i th Gaussian primitive relative to the anchor center, \mathbf{S}_2 is the scaling factor of offset and \mathbf{x} is the position of anchor in global coordinate. We illustrate the motion of anchor in Fig. 4.

$$\mathbf{p}_t^i = \mathbf{R}_t \mathbf{S}_2 \mathbf{o}^i + \mathbf{x} + \mathbf{T}_t \quad (8)$$

Here, \mathbf{o}^i , \mathbf{S}_2 and \mathbf{x} are additionally time-independent parameters to be transmitted.

3.2. Compression

Sorting-based 2D re-organization: Leveraging the alignment provided by the canonical space and deformation, our representation can be sorted and reorganized into two videos as shown in Fig. 3, allowing both temporal and spatial compression. Specifically, we map the Gaussian primitives from 3D to 2D space following [29]. While [29] is applied to static scene compression and apply sorting based on position and color, our sorting is conducted according to the position of the canonical anchors and the PCA of the time-independent features. More details can be seen in our supplementary material.

Obtaining the 2D position of each anchor, we stack the parameters of each anchor into two videos. One video $\mathbf{V}_{\text{TI}} \in \mathbb{R}^{(12+3 \times K+C) \times 1 \times H \times W}$ contains time-independent information $\{\mathbf{x} \in \mathbb{R}^3, \mathbf{S}_1 \in \mathbb{R}^3, \mathbf{S}_2 \in \mathbb{R}^3, \{\mathbf{o}_i \in \mathbb{R}^3\}_{i=1}^K, \mathbf{M} \in \mathbb{R}^3, \mathbf{f} \in \mathbb{R}^C\}$, where $(12 + 3 \times K + C)$ is the number of channels and is considered as the time dimension, and $\mathbf{M} = \{M_{de}, M_{knn}, M_{dy}\}$. The other video $\mathbf{V}_{\text{GF}} \in \mathbb{R}^{N \times P \times h \times w}$ contains time-dependent feature stream $\{\mathbf{f}_t\}_{t=1}^N$, where the video consists of N frames, each with P channels.

Observing the sparsity of the feature stream, we directly discard the feature stream set to zero by M_{de} , and reorganize remaining features by skipping over the zero using line-by-line scanning. As a result, the resolution of \mathbf{V}_{GF} becomes much smaller than that of \mathbf{V}_{TI} , i.e., $h < H$ and $w < W$. Note that we transmit M_{de} to preserve the point-wise correspondence between \mathbf{V}_{GF} and \mathbf{V}_{TI} . Following reorganization, we design an end-to-end compression method containing quantization-aware training, entropy constraint and entropy encoding. Notably, the representation trained with our entropy supervision can also be compressed using traditional video codecs, such as VVC [3] and HEVC [36].

Quantization-Aware Training: To simulate compression process, we quantize the features into integer values during training, utilizing the Straight-Through Estimator (STE):

$$\bar{\mathbf{f}} = \text{SG}(\text{round}(\mathbf{f}) - \mathbf{f}) + \mathbf{f} \quad (9)$$

where $\text{SG}()$ denotes gradient-stopping operation. This approach ensures effective feature quantization while maintaining the differentiability needed for end-to-end training.

Entropy Regularization: We use conditional entropy regularization to compress both \mathbf{V}_{TI} and \mathbf{V}_{GF} inspired by End-to-End compression methods [2, 5, 19, 24, 27]. We compress the time-dependent feature stream video \mathbf{V}_{GF} and the time-independent video \mathbf{V}_{TI} separately.

For entropy regularization of \mathbf{V}_{GF} , we exploit autoregressive probability estimation inspired by video compression methods [19, 24, 27]. Let $\mathbf{V}_{\text{GF}}^t \in \mathbb{R}^{P \times h \times w}$ denote the t th frame of \mathbf{V}_{GF} . To estimate the entropy for ev-

ery frame, we jointly train neural networks to predict the distribution of the next frame \mathbf{V}_{GF}^t with k previous frames $\{\mathbf{V}_{\text{GF}}^{t-k}, \dots, \mathbf{V}_{\text{GF}}^{t-1}\}$ as input:

$$h_{\theta}^{\text{ent}} : [\mathbf{V}_{\text{GF}}^{t-k}; \dots; \mathbf{V}_{\text{GF}}^{t-1}] \mapsto \{\boldsymbol{\mu}_t, \boldsymbol{\sigma}_t\} \quad (10)$$

where h_{θ}^{ent} is convolutional neural networks, $\boldsymbol{\mu}_t$ and $\boldsymbol{\sigma}_t$ are the predicted mean and variance of frame \mathbf{V}_{GF}^t assuming Gaussian distribution. If available previous frames are fewer than k , we directly pad the input with zeros. Based on this predicted distribution, we compute the prior probability of the next frame and subsequently estimate the entropy loss $\mathcal{L}_{\text{entropy}}$. Given the predicted $\boldsymbol{\sigma}_t$ and $\boldsymbol{\mu}_t$, the entropy loss of frame \mathbf{V}_{GF}^t is estimated as shown in Eq. 11, where $\Phi_{\boldsymbol{\sigma}_t}$ denotes the cumulative distribution function.

$$\mathcal{L}_{\text{entropy}} = - \sum_t \log(\Phi_{\boldsymbol{\mu}_t, \boldsymbol{\sigma}_t}(\mathbf{V}_{\text{GF}}^t + 0.5) - \Phi_{\boldsymbol{\mu}_t, \boldsymbol{\sigma}_t}(\mathbf{V}_{\text{GF}}^t - 0.5)) \quad (11)$$

where 0.5 indicates half of the quantization step as we quantize features into integer values.

The entropy regularization for \mathbf{V}_{TI} follows a similar approach to \mathbf{V}_{GF} . For \mathbf{f} in \mathbf{V}_{GF} , we group feature frames into fragments and perform probability estimation conditioned on the k previous fragments. The probability for the remaining attributes $\{\mathbf{x}, \mathbf{S}_1, \mathbf{S}_2, \{\mathbf{o}_i\}_{i=1}^K, \mathbf{M}\}$ in \mathbf{V}_{TI} is estimated based on \mathbf{f} , as we empirically observe that \mathbf{f} correlates with these attributes. More details can be seen in the supplementary material.

Encoding Methods: After quantization-aware training with entropy constraints, we conduct quantization and entropy coding using the learned probability distribution, typically known as end-to-end compression. Specifically, we quantize parameters with the quantization step used in training and conduct entropy encoding using rANS [7] codec.

Optionally, we can also utilize the existing video codec to conduct compression. Although the compression efficiency is lower than the end-to-end compression, their advantage lies in their widespread support and specialized hardware acceleration. Note that the quantization-aware training and entropy regularization during training also contribute to improved compression performance when using these traditional video codecs, as the distribution of the representation is constrained.

3.3. Optimization Strategy

Densification and Pruning: The densification of the vanilla Scaffold-GS [25] is directed by the gradients of parameters, which are averaged over several iterations during training. This averaging approach works well in 3D scenarios because it effectively reflects errors from different views. However, in 4D settings, this makes the gradients

averaged across time, which results in Gaussians representing fast-moving objects receiving insufficient gradients to reach the clone or split threshold. Since these Gaussians are crucial for capturing dynamic details, we modify the gradient accumulation method. Specifically, we continue to average the gradients across different views but store the gradients at different time stamps separately. For each anchor, we compute the maximum gradient value across time and then combine it with the temporal average gradient using a weight factor α . As a result, the accumulated gradients are adjusted as Eq. 12, where \mathbf{g}_t is the norm of gradients.

$$\bar{\mathbf{g}} = \alpha \max_{t \in [0,1]} (\mathbf{g}_t) + (1 - \alpha) \frac{1}{L} \sum_{t \in [0,1]} \mathbf{g}_t \quad (12)$$

For pruning, we follow CSTG to multiply each anchor’s scaling and opacity with learnable binary mask M_p , and encourage the average value of M_p to be small through regularization loss \mathcal{L}_m . If the Gaussian primitives are deemed significant, the rendering loss generates opposing gradients to preserve these primitives. Every 500 iterations, we evaluate the mask values and prune any primitives whose corresponding mask values approach zero.

Regularization and Loss Function: We train our representation with photo loss \mathcal{L}_{photo} and regularization terms. To encourage the rigidity of Gaussian primitives and encourage the sparsity of our motion-aware feature streams, we punish the parameters $M = \{M_{de}, M_{dy}, M_{knn}, M_p\}$ with regularization loss:

$$\mathcal{L}_m = |M| \quad (13)$$

To enhance the temporal consistency, we attach L1 loss to the deformed attributes \mathbf{A}_t of Gaussian primitives for adjacency timestamps:

$$\mathcal{L}_s = |\mathbf{A}_t - \mathbf{A}_{t+1}| \quad (14)$$

Following [29], we enhance the spatial smoothness of \mathbf{V}_{TI} through MSE loss \mathcal{L}_{ss} between the re-organized frames and their corresponding blurred versions. In summary, we combine all the aforementioned losses with hyper-parameters λ_e, λ_r as follows:

$$\mathcal{L} = \mathcal{L}_{photo} + \lambda_e \mathcal{L}_{entropy} + \lambda_r (\mathcal{L}_s + \mathcal{L}_{ss} + \mathcal{L}_m) \quad (15)$$

4. Experiments

4.1. Experimental Settings

Baselines: We compare our methods with the latest 4D Gaussian compression method CSTG [18] and representative methods STG [23], 4DGS [42] E-D3DGS [1], and 4DGaussian [41]. Among these, STG and 4DGS represent

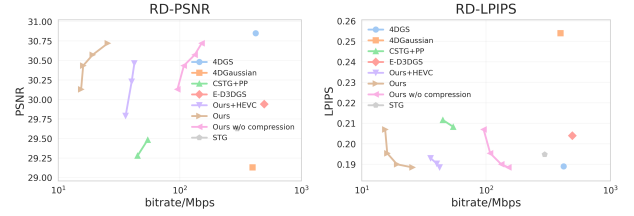


Figure 5. **RD Curve Comparison on MPEG dataset.** We visualize the RD Curve results in the **GOP 65** setting.

4D Gaussian Splatting methods, while 4DGaussian and E-D3DGS represents deformation-based methods.

Datasets: We conduct experiments on three datasets: the widely used Neur3D [22], Panoptic Sports [14] and a more challenging MPEG dataset, which is available for standardization activities related to 3DGS compression in MPEG. The Neur3D dataset comprises six indoor multi-view sequences captured by 18-21 cameras at 2704×2028 resolution. For this dataset, we follow previous methods by using half resolution for the first 300 frames. The Panoptic Sports dataset contains six sequences at 640×360 resolution, each captured from 31 cameras. Our experiments focus on two sequences: basketball and boxes. The MPEG dataset includes two indoor multi-view sequences featuring fast motion scenarios (bartending and basketball), captured by 20-30 cameras at approximately 1080p resolution. We conduct experiments on the first 65 frames at original resolution.

Metrics: We compute Rate-Distortion (RD) metrics to comprehensively evaluate different methods. For distortion evaluation, we use the PSNR, SSIM, and LPIPS [44] as the quality metrics. For representation size, we use the bitrate, consistent with standard video compression methods.

4.2. Implementation Details

Initialization: We train a Group-of-Pictures (GOP) jointly, and use the sparse point clouds as the initialization generated by COLMAP from the first frame.

Hyper-parameter and Training Process: In all experiments we set λ_r to 0.0005 and K to 5. The feature stream channel P is set to 4 for the Neur3D dataset and 8 for the MPEG dataset since the latter changes faster across time. The time-independent feature channel C is set to 48 for the “coffee martini”, “cook spinach”, and “flame salmon” scenes in the Neur3D dataset for better quality, and 24 for the remaining scenes. We train every GOP with 30K iterations and first only train canonical space for 5% iterations, and then we train the canonical space and deformation field jointly without any compression for 15% iterations. For the remaining iterations, we reorganize Gaussian primitives every 500 iterations and introduce the 2D smoothness con-

Method	Neur3D					Panoptic Sport*					MPEG				
	PSNR \uparrow	SSIM \uparrow	LPIPS (ALEX) \downarrow	FPS \uparrow	Storage (MB) \downarrow	PSNR \uparrow	SSIM \uparrow	LPIPS (VGG) \downarrow	FPS \uparrow	Storage (MB) \downarrow	PSNR \uparrow	SSIM \uparrow	LPIPS (VGG) \downarrow	FPS \uparrow	Storage (MB) \downarrow
NeRFPlayer [35]	30.69	0.932	0.111	0.05	5100	-	-	-	-	-	-	-	-	-	-
K-Planes [10]	31.63	-	-	0.30	311	-	-	-	-	-	-	-	-	-	-
Dynamic3DGS [26]	-	-	-	-	-	28.84	0.910	0.175	-	2083.8	-	-	-	-	-
4DGaussian [41]	31.15	-	0.049	30	90	27.71	0.914	0.175	55	137.7	29.13	0.866	0.254	21	108
4DGS [42]	32.01	-	-	114	202	28.68	0.911	0.157	200	973.8	30.50	0.888	0.191	80	114
E-D3DGS [1]	31.42	0.945	0.037	-	137	25.61	0.896	0.172	50	297.9	29.94	0.881	0.204	35	134
STG [23]	32.05	0.946	0.044	140	200	25.09	0.900	0.181	270	180.9	29.62	0.886	0.195	93	80
CSTG + PP [18]	31.69	0.945	0.054	186	15	26.13	0.902	0.192	360	23.4	29.48	0.885	0.208	115	15
Ours	31.75	0.938	0.051	95	10	29.50	0.931	0.114	100	12.6	30.72	0.892	0.188	70	7

Table 1. **Quantitative comparisons results.** Panoptic Sport* denotes that experiments are conducted only on two specific scenes: basketball and boxes. CSTG + PP refers to CSTG with post-processing techniques, including quantization, entropy encoding, and pruning.

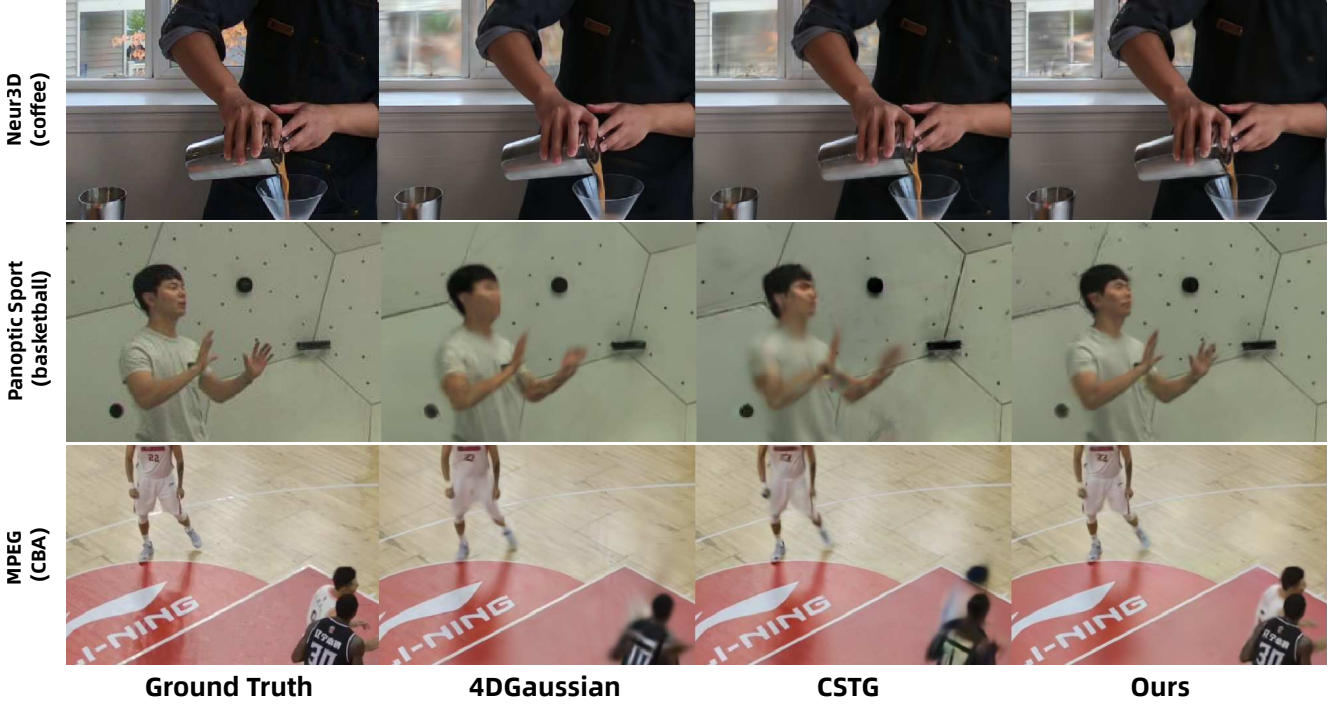


Figure 6. **Qualitative Comparison.** We implement the 4DGaussian, CSTG and compare their reconstructed quality with ours on these scenes. Our methods achieve better quality in scenes with fast motion, see the basketball player at the bottom right corner of the 3th row.

straint. Additionally, we start quantization-aware training and add entropy constraints. We adjust λ_e for the entropy loss from 0.012 to 0.00025 to obtain different bitrates for the same scene.

4.3. Comparison with State-Of-The-Art

Quantitative Evaluation: The results demonstrate that our method achieves an optimal balance between quality and storage efficiency. In terms of quality, our approach surpasses existing deformation-based methods and achieves comparable results to 4DGS methods, which model windowed spacetime regions. Furthermore, our method delivers superior quality on both the MPEG and Panoptic Sports datasets. In terms of storage requirements, our approach achieves the smallest footprint across all evaluated datasets. Although our rendering frame rate is lower than

4DGS methods, which do not require deformation calculations, our approach still delivers performance exceeding 60 FPS on a consumer-grade NVIDIA RTX 4090 graphics card.

Qualitative Evaluation: We show novel view synthesis results in Fig. 6. The first two rows demonstrate that our method is on par with existing methods on the Neur3D dataset at a small storage cost. For the MPEG datasets, 4DGaussian and CSTG struggle to model the fast motion, leading to artifacts or blurriness. In contrast, our method is capable of providing good visual quality thanks to the time-dependent features. Please refer to our supplementary material for more comparisons.

RD-Curve Comparison: To fully evaluate compression performance, we provide 4 different rate points on the datasets and visualize the RD-Curve on Fig. 5. Lower bit

Method	PSNR \uparrow	SSIM \uparrow	LPIPS \downarrow	Storage (MB) \downarrow
Full	31.94	0.879	0.190	5.3
per-frame Scaffold-GS	31.96	0.881	0.184	1283
w/o compression	32.13	0.884	0.184	46.1
w/o feature stream \mathbf{f}_t	30.59	0.867	0.208	4.4
w/o sparse mask M_{de}	31.93	0.879	0.190	6.5
w/o KNN for $\hat{\mathbf{f}}, \tilde{\mathbf{f}}_t$	31.86	0.877	0.192	5.7
w/o our densification	31.82	0.877	0.194	4.5

Table 2. **Ablation Study.** We evaluate different components in our methods on Bartender Scene.

rates can be achieved by adjusting currently fixed hyperparameters, such as the feature quantization step. The results further prove that our method achieves the optimal quality and storage balance of the rate-distortion performance.

Decoding Speed: Our decoding process includes two parts: distribution prediction and entropy decoding. Since our distribution prediction MLP h_{θ}^{ent} is tiny and the feature stream is sparse, enabling us to complete the decoding process within one second for a two-second, 30 FPS Bartender video. The feature distribution prediction can reach 100 FPS on the NVIDIA RTX4090 GPU for the Bartender scene. We use rANS to conduct entropy decoding and it reaches 5 FPS for time-independent parameters and 200 FPS for feature streams. Since we represent 65 time-stamps with a single model, the overall decoding time can be acceptable for real-time playback.

4.4. Ablation Study

We conduct ablation studies on the Bartender scene to evaluate the contribution of each component, with results shown in Table 2. We remove each part individually based on the full model. We provide a detailed memory breakdown in the supplementary material.

Compare to Scaffold-GS: We run Scaffold-GS without modifications on each frame to evaluate the representation quality and compactness of our approach (per-frame Scaffold-GS). Our observations indicate that GIFStream achieves comparable quality to this baseline while requiring only 1/200 of the storage. Furthermore, GIFStream effectively eliminates the flickering artifacts observed in per-frame Scaffold-GS.

Compression: We show the result without quantization-aware training, entropy regularization, and entropy coding (w/o compression). Here, we keep the pruning strategy of the feature streams by discarding those set to 0 by M_{de} , and prune the anchors with M_p . We discard around 83.5% feature streams and the feature stream occupies 60% storage size in the current model. We observe that the uncompressed size is 9 times larger than compressed.

Feature Stream: We evaluate the effectiveness of the fea-



Figure 7. **Ablation Study about KNN Aggregation.** We compare the visual quality of dynamic details in this figure.

ture streams by using only the time-independent feature and positional encoding of time as the input of MLPs (w/o feature stream \mathbf{f}_t). The results show a clear degradation in rendering performance, highlighting the importance of time-dependent features for capturing fast motion. Meanwhile, storage remains largely unaffected, as the feature stream is sparse and further compressed into a small size.

Motion Mask: Next, we remove the mask M_{de} and maintain all the feature streams (w/o sparse mask M_{de}). In this experiment, the bit rate of the feature stream increases around 80% (from 1.5 MB to 2.7 MB), indicating the importance of sparse mask M_{de} .

KNN Aggregation: We further investigate the KNN feature aggregation by using $\hat{\mathbf{f}}, \tilde{\mathbf{f}}_t$ for the motion prediction head h_{θ}^{mot} (w/o KNN for $\hat{\mathbf{f}}, \tilde{\mathbf{f}}_t$). While this modification results in only a minor drop in rendering performance in quantitative metrics, it leads to noticeable visual distortion as shown in Fig. 7. Additionally, we observe an increase in storage requirements, as the number of primitives grows without the regularization provided by KNN.

Densification: Finally, we apply the densification strategy of Scaffold-GS and demonstrate that the rendering performance drops without using our densification strategy (w/o our densification). This is indicated by smaller storage requirements and fewer Gaussians being inserted when averaging the gradients across the time dimension.

5. Conclusion

We propose to incorporate a sparse feature stream to deformation-based 4D Gaussian representation, enabling capturing highly dynamic content and efficient temporal compression for time-dependent content. We also design end-to-end compression methods for our representation making the 3DGS-based immersive video’s bit rate comparable to 4K 2D videos. Experiments show that our representation achieves the best rate and distortion performance compared to baseline methods, and our decoding speed is acceptable for real-time immersive video watching experience. This evidence demonstrates that our method provides a promising solution for future immersive video.

Acknowledgements

This work is supported by the National Natural Science Foundation of China under Grant No. 62441223, No. 62202418 and No. U21B2004. Yiyi Liao and Lu Yu are with Zhejiang Provincial Key Laboratory of Information Processing, Communication and Networking (IPCAN), Hangzhou 310007, China.

References

- [1] Jeongmin Bae, Seoha Kim, Youngsik Yun, Hahyun Lee, Gun Bang, and Youngjung Uh. Per-gaussian embedding-based deformation for deformable 3d gaussian splatting. *arXiv preprint arXiv:2404.03613*, 2024. 1, 2, 4, 6, 7
- [2] Johannes Ballé, David Minnen, Saurabh Singh, Sung Jin Hwang, and Nick Johnston. Variational image compression with a scale hyperprior. *arXiv preprint arXiv:1802.01436*, 2018. 5
- [3] Benjamin Bross, Ye-Kui Wang, Yan Ye, Shan Liu, Jianle Chen, Gary J Sullivan, and Jens-Rainer Ohm. Overview of the versatile video coding (vvc) standard and its applications. *IEEE Transactions on Circuits and Systems for Video Technology*, 31(10):3736–3764, 2021. 5
- [4] Ang Cao and Justin Johnson. Hexplane: A fast representation for dynamic scenes. pages 130–141, 2023. 2
- [5] Yihang Chen, Qianyi Wu, Weiyo Lin, Mehrtash Harandi, and Jianfei Cai. Hac: Hash-grid assisted context for 3d gaussian splatting compression. In *European Conference on Computer Vision*, pages 422–438. Springer, 2025. 3, 5, 1
- [6] Yuanxing Duan, Fangyin Wei, Qiyu Dai, Yuhang He, Wenzheng Chen, and Baoquan Chen. 4d-rotor gaussian splatting: towards efficient novel view synthesis for dynamic scenes. In *ACM SIGGRAPH 2024 Conference Papers*, pages 1–11, 2024. 1, 2
- [7] Jarek Duda. Asymmetric numeral systems: entropy coding combining speed of huffman coding with compression rate of arithmetic coding. *arXiv preprint arXiv:1311.2540*, 2013. 5
- [8] Zhiwen Fan, Kevin Wang, Kairun Wen, Zehao Zhu, De-jia Xu, and Zhangyang Wang. Lightgaussian: Unbounded 3d gaussian compression with 15x reduction and 200+ fps. *arXiv preprint arXiv:2311.17245*, 2023. 3, 1
- [9] Sara Fridovich-Keil, Giacomo Meanti, Frederik Rahbæk Warburg, Benjamin Recht, and Angjoo Kanazawa. K-planes: Explicit radiance fields in space, time, and appearance. In *Proceedings of the IEEE/CVF Conference on Computer Vision and Pattern Recognition*, pages 12479–12488, 2023. 2
- [10] Sara Fridovich-Keil, Giacomo Meanti, Frederik Rahbæk Warburg, Benjamin Recht, and Angjoo Kanazawa. K-planes: Explicit radiance fields in space, time, and appearance. pages 12479–12488, 2023. 7
- [11] Quankai Gao, Qiangeng Xu, Zhe Cao, Ben Mildenhall, Wen-chao Ma, Le Chen, Danhang Tang, and Ulrich Neumann. Gaussianflow: Splatting gaussian dynamics for 4d content creation. *arXiv preprint arXiv:2403.12365*, 2024. 1, 2, 4
- [12] Sharath Girish, Kamal Gupta, and Abhinav Shrivastava. Eagles: Efficient accelerated 3d gaussians with lightweight encodings. *arXiv preprint arXiv:2312.04564*, 2023. 3, 1
- [13] Yi-Hua Huang, Yang-Tian Sun, Ziyi Yang, Xiaoyang Lyu, Yan-Pei Cao, and Xiaojuan Qi. Sc-gs: Sparse-controlled gaussian splatting for editable dynamic scenes. In *Proceedings of the IEEE/CVF Conference on Computer Vision and Pattern Recognition*, pages 4220–4230, 2024. 1, 2, 4
- [14] Hanbyul Joo, Hao Liu, Lei Tan, Lin Gui, Bart Nabbe, Iain Matthews, Takeo Kanade, Shohei Nobuhara, and Yaser Sheikh. Panoptic studio: A massively multiview system for social motion capture. In *Proceedings of the IEEE international conference on computer vision*, pages 3334–3342, 2015. 6
- [15] Bernhard Kerbl, Georgios Kopanas, Thomas Leimkühler, and George Drettakis. 3d gaussian splatting for real-time radiance field rendering. *ACM Trans. Graph.*, 42(4):139–1, 2023. 1
- [16] Agelos Kratimenos, Jiahui Lei, and Kostas Daniilidis. Dynmf: Neural motion factorization for real-time dynamic view synthesis with 3d gaussian splatting. In *European Conference on Computer Vision*, pages 252–269. Springer, 2025. 1, 2, 4
- [17] Joo Chan Lee, Daniel Rho, Xiangyu Sun, Jong Hwan Ko, and Eunbyung Park. Compact 3d gaussian representation for radiance field. In *Proceedings of the IEEE/CVF Conference on Computer Vision and Pattern Recognition*, pages 21719–21728, 2024. 3, 1
- [18] Joo Chan Lee, Daniel Rho, Xiangyu Sun, Jong Hwan Ko, and Eunbyung Park. Compact 3d gaussian splatting for static and dynamic radiance fields. *arXiv preprint arXiv:2408.03822*, 2024. 3, 6, 7, 1
- [19] Jiahao Li, Bin Li, and Yan Lu. Deep contextual video compression. *Advances in Neural Information Processing Systems*, 34:18114–18125, 2021. 5
- [20] Lingzhi Li, Zhen Shen, Zhongshu Wang, Li Shen, and Liefeng Bo. Compressing volumetric radiance fields to 1 mb. pages 4222–4231, 2023. 3
- [21] Sicheng Li, Hao Li, Yiyi Liao, and Lu Yu. Nerfcodec: Neural feature compression meets neural radiance fields for memory-efficient scene representation. In *Proceedings of the IEEE/CVF Conference on Computer Vision and Pattern Recognition*, pages 21274–21283, 2024. 3
- [22] Tianye Li, Mira Slavcheva, Michael Zollhoefer, Simon Green, Christoph Lassner, Changil Kim, Tanner Schmidt, Steven Lovegrove, Michael Goesele, Richard Newcombe, et al. Neural 3d video synthesis from multi-view video. In *Proceedings of the IEEE/CVF Conference on Computer Vision and Pattern Recognition*, pages 5521–5531, 2022. 2, 6
- [23] Zhan Li, Zhang Chen, Zhong Li, and Yi Xu. Spacetime gaussian feature splatting for real-time dynamic view synthesis. In *Proceedings of the IEEE/CVF Conference on Computer Vision and Pattern Recognition*, pages 8508–8520, 2024. 1, 2, 6, 7, 3
- [24] Guo Lu, Wanli Ouyang, Dong Xu, Xiaoyun Zhang, Chunlei Cai, and Zhiyong Gao. Dvc: An end-to-end deep video compression framework. In *Proceedings of the IEEE/CVF conference on computer vision and pattern recognition*, pages 11006–11015, 2019. 5

- [25] Tao Lu, Mulin Yu, Linning Xu, Yuanbo Xiangli, Limin Wang, Dahua Lin, and Bo Dai. Scaffold-gs: Structured 3d gaussians for view-adaptive rendering. In *Proceedings of the IEEE/CVF Conference on Computer Vision and Pattern Recognition*, pages 20654–20664, 2024. [2](#), [5](#)
- [26] Jonathon Luiten, Georgios Kopanas, Bastian Leibe, and Deva Ramanan. Dynamic 3d gaussians: Tracking by persistent dynamic view synthesis. In *2024 International Conference on 3D Vision (3DV)*, pages 800–809. IEEE, 2024. [7](#)
- [27] Fabian Mentzer, George Toderici, David Minnen, Sung-Jin Hwang, Sergi Caelles, Mario Lucic, and Eirikur Agustsson. Vct: A video compression transformer. *arXiv preprint arXiv:2206.07307*, 2022. [5](#)
- [28] Ben Mildenhall, Pratul P Srinivasan, Matthew Tancik, Jonathan T Barron, Ravi Ramamoorthi, and Ren Ng. Nerf: Representing scenes as neural radiance fields for view synthesis. 2020. [2](#)
- [29] Wieland Morgenstern, Florian Barthel, Anna Hilsmann, and Peter Eisert. Compact 3d scene representation via self-organizing gaussian grids. *arXiv preprint arXiv:2312.13299*, 2023. [3](#), [5](#), [6](#), [1](#)
- [30] KL Navaneet, Kossar Pourahmadi Meibodi, Soroush Abbasi Koohpayegani, and Hamed Pirsiavash. Compact3d: Compressing gaussian splat radiance field models with vector quantization. *arXiv preprint arXiv:2311.18159*, 2023.
- [31] Simon Niedermayr, Josef Stumpfegger, and Rüdiger Westermann. Compressed 3d gaussian splatting for accelerated novel view synthesis. In *Proceedings of the IEEE/CVF Conference on Computer Vision and Pattern Recognition*, pages 10349–10358, 2024. [3](#), [1](#)
- [32] Albert Pumarola, Enric Corona, Gerard Pons-Moll, and Francesc Moreno-Noguer. D-nerf: Neural radiance fields for dynamic scenes. In *Proceedings of the IEEE/CVF Conference on Computer Vision and Pattern Recognition*, pages 10318–10327, 2021. [2](#)
- [33] Daniel Rho, Byeonghyeon Lee, Seungtae Nam, Joo Chan Lee, Jong Hwan Ko, and Eunbyung Park. Masked wavelet representation for compact neural radiance fields. pages 20680–20690, 2023. [3](#)
- [34] Seungjoo Shin and Jaesik Park. Binary radiance fields. 2023. [3](#)
- [35] Liangchen Song, Anpei Chen, Zhong Li, Zhang Chen, Lele Chen, Junsong Yuan, Yi Xu, and Andreas Geiger. Nerf-player: A streamable dynamic scene representation with decomposed neural radiance fields. *IEEE Transactions on Visualization and Computer Graphics*, 29(5):2732–2742, 2023. [2](#), [7](#)
- [36] Gary J Sullivan, Jens-Rainer Ohm, Woo-Jin Han, and Thomas Wiegand. Overview of the high efficiency video coding (hevc) standard. *IEEE Transactions on circuits and systems for video technology*, 22(12):1649–1668, 2012. [5](#)
- [37] Towaki Takikawa, Alex Evans, Jonathan Tremblay, Thomas Müller, Morgan McGuire, Alec Jacobson, and Sanja Fidler. Variable bitrate neural fields. pages 1–9, 2022. [3](#)
- [38] Liao Wang, Qiang Hu, Qihan He, Ziyu Wang, Jingyi Yu, Tinne Tuytelaars, Lan Xu, and Minye Wu. Neural residual radiance fields for streamably free-viewpoint videos. In *Proceedings of the IEEE/CVF Conference on Computer Vision and Pattern Recognition*, pages 76–87, 2023. [3](#)
- [39] Liao Wang, Kaixin Yao, Chengcheng Guo, Zhirui Zhang, Qiang Hu, Jingyi Yu, Lan Xu, and Minye Wu. Videorf: Rendering dynamic radiance fields as 2d feature video streams. In *Proceedings of the IEEE/CVF Conference on Computer Vision and Pattern Recognition*, pages 470–481, 2024. [3](#)
- [40] Penghao Wang, Zhirui Zhang, Liao Wang, Kaixin Yao, Siyuan Xie, Jingyi Yu, Minye Wu, and Lan Xu. V³: Viewing volumetric videos on mobiles via streamable 2d dynamic gaussians. *arXiv preprint arXiv:2409.13648*, 2024. [3](#)
- [41] Guanjun Wu, Taoran Yi, Jiemin Fang, Lingxi Xie, Xiaopeng Zhang, Wei Wei, Wenyu Liu, Qi Tian, and Xinggang Wang. 4d gaussian splatting for real-time dynamic scene rendering. In *Proceedings of the IEEE/CVF Conference on Computer Vision and Pattern Recognition*, pages 20310–20320, 2024. [1](#), [2](#), [4](#), [6](#), [7](#)
- [42] Zeyu Yang, Hongye Yang, Zijie Pan, and Li Zhang. Real-time photorealistic dynamic scene representation and rendering with 4d gaussian splatting. *arXiv preprint arXiv:2310.10642*, 2023. [1](#), [2](#), [6](#), [7](#)
- [43] Ziyi Yang, Xinyu Gao, Wen Zhou, Shaohui Jiao, Yuqing Zhang, and Xiaogang Jin. Deformable 3d gaussians for high-fidelity monocular dynamic scene reconstruction. In *Proceedings of the IEEE/CVF Conference on Computer Vision and Pattern Recognition*, pages 20331–20341, 2024. [1](#), [2](#), [4](#)
- [44] Richard Zhang, Phillip Isola, Alexei A. Efros, Eli Shechtman, and Oliver Wang. The unreasonable effectiveness of deep features as a perceptual metric. 2018. [6](#)
- [45] Xinjie Zhang, Zhening Liu, Yifan Zhang, Xingtong Ge, Dailan He, Tongda Xu, Yan Wang, Zehong Lin, Shuicheng Yan, and Jun Zhang. Mega: Memory-efficient 4d gaussian splatting for dynamic scenes. *arXiv preprint arXiv:2410.13613*, 2024. [3](#)

GIFStream: 4D Gaussian-based Immersive Video with Feature Stream

Supplementary Material

1. Overview

In this supplementary material, we present three sections: (I) additional details on the methods, (II) supplementary information on the experiments, and (III) a discussion of limitations and future work.

2. Supplementary for Methods

Details on 3D-to-2D Sorting: We adopt the sorting strategy introduced in PLAS [29] to reorganize the Gaussian primitives from 3D space to 2D space based on the similarity of their attributes. While [29] sorts static 3D Gaussian primitives using their positions, zero-degree spherical harmonic (SH) coefficients, and scaling, we sort our canonical anchors based on their positions and the three principal components of the time-independent features \mathbf{f} obtained through Principal Component Analysis (PCA). All the parameters used for sorting are normalized to the range $[0, 1]$ along the channel dimension through min-max normalization.

Compression for Time-Independent Video: Our time-independent video \mathbf{V}_{TI} , comprises two components: time-independent features frames and other attributes frames, including $\mathbf{x}, \mathbf{S}_1, \mathbf{S}_2, \{\mathbf{o}^i\}, M$. For compressing this video, there are many options, including existing 3DGS compression methods [5, 8, 12, 17, 29–31] and our feature stream compression methods. We perform compression following the same principle as compressing the time-dependent video to keep our overall method simple and effectively exploit intra-channel and spatial dependencies.

We compress the features frames in an auto-regressive manner, grouping the frames into n fragments, $\{\mathbf{F}_i\}_{i=1}^n$, and predicting their distribution as described in Eq. (16). This compression method effectively leverages both the channel and spatial dependencies of the anchors, as convolutional networks h_ϕ^{ent2} are employed to predict the conditional distribution.

$$h_\theta^{\text{ent2}} : [\mathbf{F}_{i-k}; \dots; \mathbf{F}_{i-1}] \mapsto \{\mu_i, \sigma_i\} \quad (16)$$

We compress the $\mathbf{S}_1, \mathbf{S}_2, \{\mathbf{o}^i\}, M$ with the per-parameter distribution and adaptive quantization steps \mathbf{Q} predicted from time-independent feature $\tilde{\mathbf{f}}$ using neural network h_ϕ^{ent3} :

$$h_\theta^{\text{ent3}} : [\tilde{\mathbf{f}}] \mapsto \{\mu, \sigma, \mathbf{Q}\} \quad (17)$$

The quantization of $\mathbf{S}_1, \mathbf{S}_2, \{\mathbf{o}^i\}, M$ is performed using the Straight-Through Estimator (STE):

$$\bar{\mathbf{A}} = \text{SG}(\text{round}(\mathbf{A}/Q) - \mathbf{A}/Q) \times Q + \mathbf{A} \quad (18)$$

Methods	Rate	Scenes	PSNR \uparrow	SSIM \uparrow	LPIPS (VGG) \downarrow	Storage (MB) \downarrow
4DGS	rate0	Bartender	31.58	0.865	0.221	126.2
		CBA	29.43	0.911	0.161	101.6
		AVG	30.50	0.888	0.191	113.9
4DGaussian	rate0	Bartender	31.06	0.858	0.249	108.0
		CBA	27.2	0.875	0.259	107.0
		AVG	29.13	0.867	0.254	107.5
STG	rate0	Bartender	31.4	0.875	0.207	49.1
		CBA	27.85	0.896	0.183	111.3
		AVG	29.63	0.886	0.195	80.2
CSTG	rate0	Bartender	31.12	0.876	0.218	10.7
		CBA	27.85	0.895	0.199	18.8
		AVG	29.48	0.885	0.208	14.7
	rate1	Bartender	31.06	0.874	0.221	8.2
		CBA	27.5	0.892	0.202	16.2
		AVG	29.28	0.883	0.212	12.2
Ours	rate0	Bartender	31.94	0.879	0.190	5.3
		CBA	29.5	0.906	0.187	8.5
		AVG	30.72	0.893	0.189	6.9
	rate1	Bartender	31.69	0.876	0.195	3.3
		CBA	29.46	0.906	0.185	7.1
		AVG	30.57	0.891	0.190	5.2
	rate2	Bartender	31.48	0.873	0.201	2.6
		CBA	29.39	0.905	0.190	6.1
		AVG	30.43	0.889	0.195	4.3
	rate3	Bartender	31.35	0.872	0.207	2.3
		CBA	28.91	0.897	0.207	6.1
		AVG	30.13	0.885	0.207	4.2

Table 3. **Per-Scene Results on The MPEG dataset.** We present the PSNR, SSIM, LPIPS (VGG), and storage result of each methods.

Here, \mathbf{A} represents the attributes in $\mathbf{S}_1, \mathbf{S}_2, \{\mathbf{o}^i\}, M$ and SG denotes the stop gradient operation. The entropy loss for \mathbf{A} is similar to that of \mathbf{V}_{GF} , but the half quantization step is modified from 0.5 to $Q/2$.

For the position \mathbf{x} of anchors, we simply apply 16-bit quantization and store the results as a PNG image.

3. Supplementary for Experiments

Additional Implementation Details: We implement 4DGaussian, 4DGS, STG and CSTG [18, 23, 41, 42] using their official code bases. For the 4DGS, we only keep zero degrees of SH coefficients, therefore the storage will be much smaller than the original version. For the Neur3D dataset, we directly cite reported results from CSTG [18] in our paper. For the MPEG dataset, as no predefined hyper-parameters are available, we conduct multiple experiments with various hyper-parameter combinations, adjusted from the Neur3D configurations, and select the best-performing ones as our comparison benchmarks.

To obtain multi-rate results for CSTG on the MPEG dataset, we adjust the weight of the loss function associated with the pruning mask.

Per-Scene Quantitative Comparison: Detailed per-scene

Experiment	Scenes	Time-independent Feature \mathbf{f} (MB)	Attributes (MB)	Time-dependent Feature \mathbf{f}_t (MB)	Neural networks (MB)
GIFStream w/ Compression	Bartender	0.79	2.85	1.46	0.1
	CBA	1.47	5.62	2.88	0.1
	AVG	1.13	4.23	2.17	0.1
GIFStream w/o Compression	Bartender	18.68		27.42	0.1
GIFStream w/o Sparse Mask M_{de}	Bartender	0.88	2.89	2.68	0.1

Table 4. **Memory Breakdown.** For a more comprehensive evaluation, we present the memory breakdown for each experiment. In the GIFStream w/o Compression experiment, we provide the total memory usage of the time-independent features and attributes.

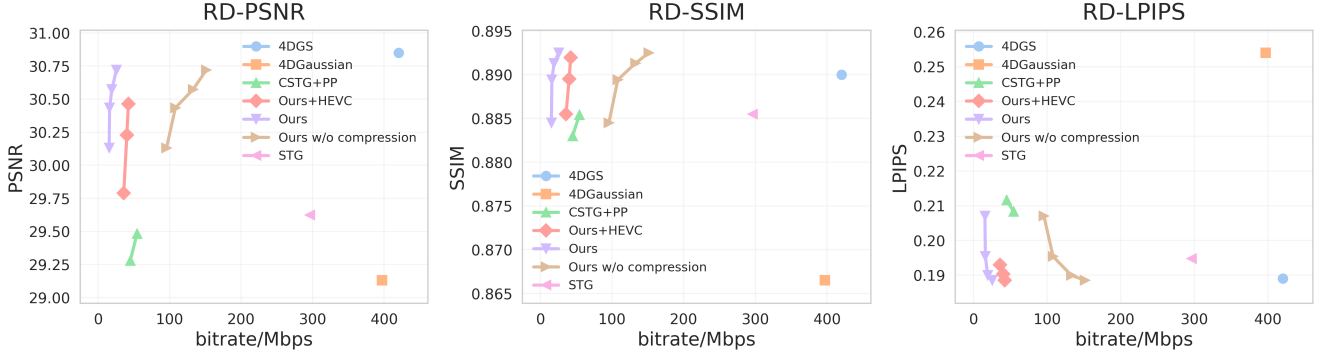


Figure 8. **RD Curve Comparison on MPEG dataset.** We visualize the RD Curve results in the **GOP 65** setting.

results for the Neur3D dataset are provided in Table 5, and detailed per-scene results for the MPEG dataset are provided in Table 3.

More Qualitative Evaluation: We provide additional qualitative results in Fig. 10 and Fig. 9 for better evaluation. To accurately segment the video into complete GOPs, We train GIFStream with a GOP of 60 for the Neur3D dataset and with a GOP of 65 for the MPEG dataset. Additionally, we observe flicker across different GOPs in the static background of the scenes like “flame salmon 1”, since the reconstruction of content out of windows is challenging and artifacts in these areas look different in different GOPs. To improve the temporal consistency of these scenes, we utilize the previous GOP as initialization for the next GOP. Specifically, we load the checkpoint from the previous GOP and start training from the 10000th iteration for 10 minutes. During this process, we add and remove points to accommodate new content.

Memory Break Down: We provide the memory breakdown for parts of our experiments in Table 4. This includes the memory usage of the compressed GIFStream using our end-to-end compression (GIFStream w/ Compression) and the uncompressed GIFStream, which is trained without compression techniques (GIFStream w/o Compression). Additionally, we present the increase in memory requirements when sparse feature masks are not applied (GIFStream w/o Sparse Mask M_{de}).

Scenes	PSNR \uparrow	SSIM \uparrow	LPIPS \downarrow	Storage (MB) \downarrow
coffee martini	28.14	0.905	0.163	11.1
cook spinach	33.03	0.950	0.138	12.0
cut roasted beef	33.19	0.947	0.141	8.8
flame salmon 1	28.51	0.916	0.157	8.2
flame steak	33.76	0.957	0.134	8.2
sear steak	33.83	0.958	0.134	10.2

Table 5. **Per-Scene Results on The Neur3D dataset.** We present the specific results of each scene on the Neur3D dataset.

Compression Utilizing HEVC: We perform simple compression utilizing image and video compression codecs on the MPEG dataset and present the RD-Curve in Fig. 8. Specifically, we apply 16-bit quantization to the attributes $\mathbf{x}, \mathbf{S}_1, \mathbf{S}_2, \{\mathbf{o}^i\}_{i=1}^K, \mathbf{M}$ and 8-bit quantization for the feature \mathbf{f} and \mathbf{f}_t . Subsequently, we use PNG compression for $\mathbf{x}, \mathbf{S}_1, \mathbf{S}_2, \{\mathbf{o}^i\}_{i=1}^K, \mathbf{M}, \mathbf{f}$ and employ HEVC to compress \mathbf{f}_t . While being inferior to our end-to-end compression solution, the HEVC-based compression also yields promising performance compared with other baselines. This demonstrates that our proposed feature streams are also compatible with existing video codecs.

4. Limitation

Our representation may exhibit inconsistencies in the background area between different GOPs, particularly in the distant background, where there are insufficient points for ini-



Figure 9. **More Qualitative Evaluation.** We present complete frames from the MPEG dataset along with a comparison of local details in this figure.

tialization. This is due to the instability of densification. The adaptive sampling strategy from STG [23] or the continual training approach can help alleviate this issue. Additionally, since our representation and compression methods require neural networks for inference, the computational demands may be unacceptable for some mobile devices.

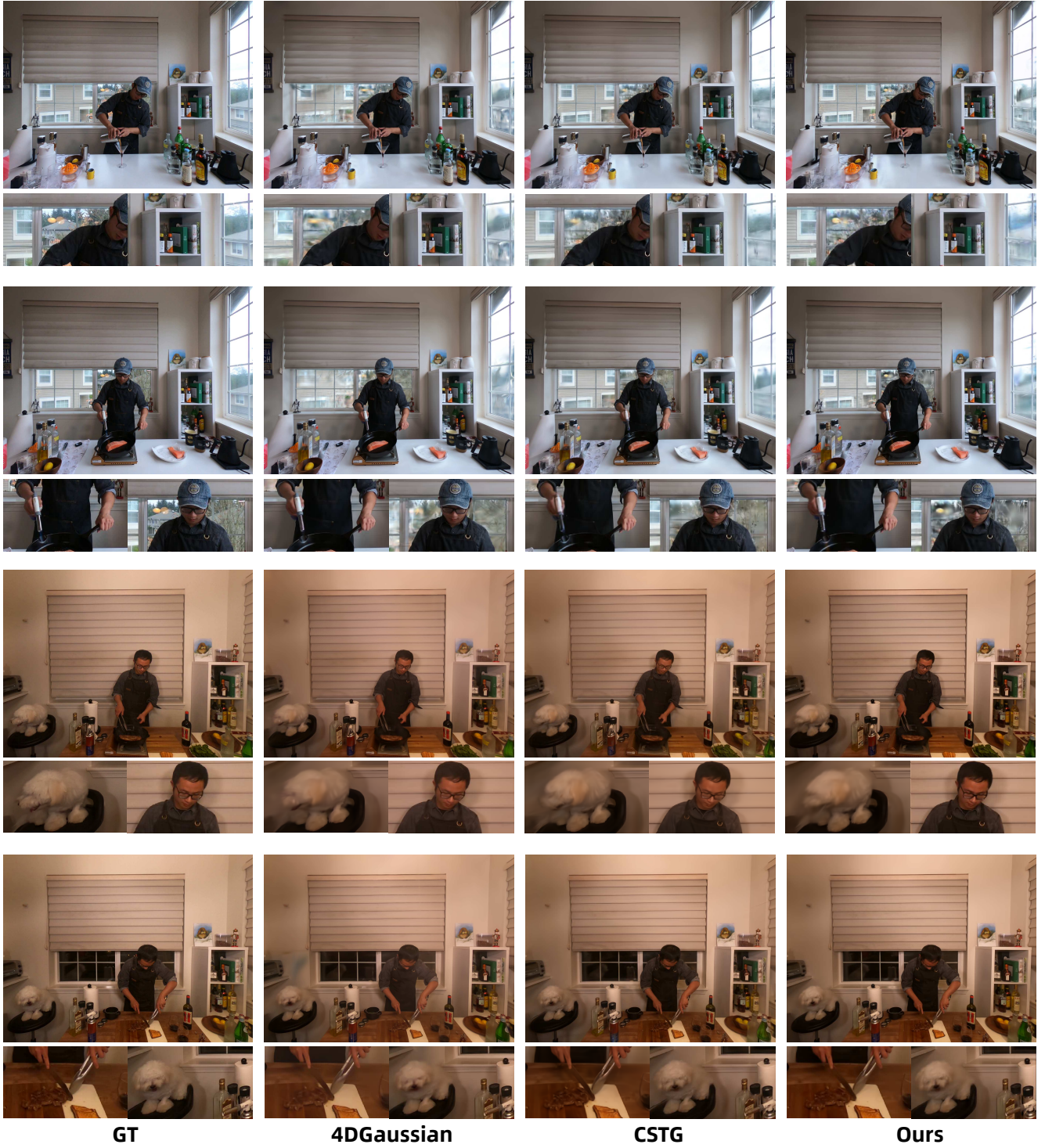


Figure 10. **More Qualitative Evaluation.** We present complete frames from the Neur3D dataset along with a comparison of local details in this figure.